

## A spectroscopic study of the surfaces of Saturn's large satellites: H<sub>2</sub>O ice, tholins, and minor constituents <sup>☆</sup>

Dale P. Cruikshank <sup>a,\*</sup>, Tobias C. Owen <sup>b</sup>, Cristina Dalle Ore <sup>a,c</sup>, Thomas R. Geballe <sup>d</sup>,  
Ted L. Roush <sup>a</sup>, Catherine de Bergh <sup>e</sup>, Scott A. Sandford <sup>a</sup>, Francois Poulet <sup>f</sup>,  
Gretchen K. Benedix <sup>g</sup>, Joshua P. Emery <sup>a,c</sup>

<sup>a</sup> NASA Ames Research Center, 245-6, Moffett Field, CA 94035-1000, USA

<sup>b</sup> Institute for Astronomy, University of Hawaii, 2680 Woodlawn Dr., Honolulu, HI 96822, USA

<sup>c</sup> SETI Institute, 2035 Landings Dr., Mountain View, CA 94043, USA

<sup>d</sup> Gemini Observatory, 670 N. A'ohoku Pl., Hilo, HI 96720, USA

<sup>e</sup> Observatoire de Paris, 5 Place Jules Janssen, Meudon Cedex 92195, France

<sup>f</sup> Institut d'Astrophysique Spatiale, Bât. 121, Université de Paris-Sud, F91405 Orsay Cedex, France

<sup>g</sup> Department of Earth and Planetary Sciences, Washington University, St. Louis, MO 63130, USA

Received 8 August 2003; revised 30 August 2004

Available online 2 March 2005

### Abstract

We present spectra of Saturn's icy satellites Mimas, Enceladus, Tethys, Dione, Rhea, and Hyperion, 1.0–2.5  $\mu\text{m}$ , with data extending to shorter (Mimas and Enceladus) and longer (Rhea and Dione) wavelengths for certain objects. The spectral resolution ( $R = \lambda/\Delta\lambda$ ) of the data shown here is in the range 800–1000, depending on the specific instrument and configuration used; this is higher than the resolution ( $R = 225$  at 3  $\mu\text{m}$ ) afforded by the Visual-Infrared Mapping Spectrometer on the Cassini spacecraft. All of the spectra are dominated by water ice absorption bands and no other features are clearly identified. Spectra of all of these satellites show the characteristic signature of hexagonal H<sub>2</sub>O ice at 1.65  $\mu\text{m}$ . We model the leading hemisphere of Rhea in the wavelength range 0.3–3.6  $\mu\text{m}$  with the Hapke and the Shkuratov radiative transfer codes and discuss the relative merits of the two approaches to fitting the spectrum. In calculations with both codes, the only components used are H<sub>2</sub>O ice, which is the dominant constituent, and a small amount of tholin (Ice Tholin II). Tholin in small quantities (few percent, depending on the mixing mechanism) appears to be an essential component to give the basic red color of the satellite in the region 0.3–1.0  $\mu\text{m}$ . The quantity and mode of mixing of tholin that can produce the intense coloration of Rhea and other icy satellites has bearing on its likely presence in many other icy bodies of the outer Solar System, both of high and low geometric albedos. Using the modeling codes, we also establish detection limits for the ices of CO<sub>2</sub> (a few weight percent, depending on particle size and mixing), CH<sub>4</sub> (same), and NH<sub>4</sub>OH (0.5 weight percent) in our globally averaged spectra of Rhea's leading hemisphere. New laboratory spectral data for NH<sub>4</sub>OH are presented for the purpose of detection on icy bodies. These limits for CO<sub>2</sub>, CH<sub>4</sub>, and NH<sub>4</sub>OH on Rhea are also applicable to the other icy satellites for which spectra are presented here. The reflectance spectrum of Hyperion shows evidence for a broad, unidentified absorption band centered at 1.75  $\mu\text{m}$ .

© 2004 Elsevier Inc. All rights reserved.

**Keywords:** Ices; Infrared observations; Satellites of Saturn; Spectroscopy; Surfaces, satellite; Organic chemistry

<sup>☆</sup> The authors dedicate this paper to the memory of a friend and colleague, Vasily Ivanovich Moroz (1931–2004), one of founders of modern planetary physics and a pioneer in infrared spectroscopy of Solar System bodies.

\* Corresponding author. Fax: +1-650-604-6779.

E-mail address: [dale.p.cruikshank@nasa.gov](mailto:dale.p.cruikshank@nasa.gov) (D.P. Cruikshank).

## 1. Introduction

It is well established from near-infrared (1.0–2.5  $\mu\text{m}$ ) spectroscopy that the surfaces of Saturn's major airless satellites—with the possible exception of the low-albedo (leading) hemisphere (LH) of Iapetus—are predominantly covered by water ice (e.g., Fink et al., 1976; Clark et al., 1984; Roush et al., 1995; Cruikshank et al., 1998a). The reflectance spectra show several characteristic absorption bands of H<sub>2</sub>O ice, plus the 1.65- $\mu\text{m}$  absorption band characteristic of hexagonal ice at low temperature, first recognized in Saturn's rings (Kuiper et al., 1970; Pilcher et al., 1970; Fink and Larson, 1975; Fink and Sill, 1982). Kuiper (1957) was the first to propose that ice must be present in the rings from his unpublished observations, while near-infrared spectra obtained in 1964 by Moroz (1967, Fig. 191) clearly show H<sub>2</sub>O ice absorption. Reviews of the discoveries of ice on Saturn's satellites have been presented by Cruikshank et al. (1984), Clark et al. (1986), and Cruikshank et al. (1998a), while the full story of the detection of ice absorptions in spectra of the rings has not yet been written. A recent and comprehensive study of the near-infrared spectra of the rings has been published by Poulet et al. (2003). Further historical details are beyond the scope of this paper.

Models for the interiors of these satellites indicate that they must be composed of mixtures of ice and denser materials (presumably rock plus organic compounds) in varying proportions (e.g., Lupo and Lewis, 1979; Schubert et al., 1986). Morphological evidence of internal geological activity on some of these objects, plus models for their formation from a Saturn subnebula have fueled speculation that other compounds besides ice may be present on the surface, notably ammonia hydrate (Prinn and Fegley, 1981; Smith et al., 1981; Morrison et al., 1986). The outer regular satellites (beyond Titan), however, may have accreted in regions of the disk that are disconnected from the inner portions where disk conditions would have led to the formation of such compounds (Mosqueira and Estrada, 2003a). A possible absorption band at 1.85  $\mu\text{m}$  reported in spectra of the trailing hemisphere of Tethys by Clark et al. (1984) would indicate the presence of something besides water ice if it were confirmed, and UV studies with HST have demonstrated the presence of O<sub>3</sub> and a possible organic compound on Dione and Rhea (Noll et al., 1997). In the cases of Hyperion, Phoebe, and the low-albedo hemisphere of Iapetus, it is obvious that other materials *must* be present, darkening the surfaces and producing a strong reddening of the visible spectra of Hyperion and the leading hemisphere of Iapetus (Clark et al., 1984; Roush et al., 1995; Cruikshank et al., 1998a). Ice was only recently detected on Phoebe (Owen et al., 1999; Brown, 2000).

Because of a general tendency for ageing effects to darken surfaces of solid bodies in the Solar System, the high albedos of Mimas, Enceladus, Tethys, Dione, and Rhea invite further study. In view of their albedos, the range of densities (0.98–1.49 g cm<sup>-3</sup>) among these satellites is also note-

worthy (Smith et al., 1981). These satellites may have undergone a unique formation history. A recent study (Mosqueira and Estrada, 2003b) has them forming 10<sup>4</sup>–10<sup>5</sup> years after the formation of Titan, at a time when gas dissipation was taking place, the disk was becoming optically thin, and most of the silicates in the disk had been lost to the planet by gas drag. Hence, it is important to constrain the physical properties of the satellites, including their surface compositions.

For these and other reasons, we undertook a spectroscopic study of Saturn's largest icy satellites, using the cooled grating spectrometer CGS4 at the United Kingdom Infrared Telescope (UKIRT) (Mountain et al., 1990). Additional data for Rhea, Enceladus, and Mimas were obtained using the SpeX spectrometer (Rayner et al., 2003). The CGS4 data were obtained in individual spectral segments of 0.15–0.64  $\mu\text{m}$  that were also separated in time, while the SpeX data were obtained simultaneously over the region 0.8–2.5  $\mu\text{m}$  in several orders of a cross-dispersed echelle. Our study of the low-albedo hemisphere of Iapetus has been reported by Owen et al. (2001), and our Phoebe study appears in Owen et al. (1999). In this paper, we present additional results from this program.

## 2. Observations and models

We observed the trailing hemispheres (TH) of Mimas and Tethys, the leading hemisphere (LH) of Enceladus, and both hemispheres of Dione and Rhea. The chaotic rotation of Hyperion precludes the possibility of defining a leading/trailing hemisphere spectrum. We recorded the spectra of these objects in the region 0.8–2.5  $\mu\text{m}$ , with the best quality data primarily in the region 1.4–2.5  $\mu\text{m}$ . The spectra of Dione and Rhea were observed to a long wavelength limit of 3.6  $\mu\text{m}$ . The relevant parameters describing these observations are given in Table 1. All of the data were obtained with the CGS4 spectrometer on UKIRT, except as noted.

### 2.1. Rhea

We observed Rhea with the UKIRT/CGS4 and the IRTF/SpeX, covering the region 0.8–3.6  $\mu\text{m}$  for a fraction of the satellite's surface that corresponds primarily to the leading hemisphere. The data shown in Fig. 1 consist of segments of the spectrum that were obtained at different times and different positions on Rhea's surface, as noted in Table 1. The variations in albedos and strength of spectral features with position on the satellite's surface can easily account for the different levels and small mismatches seen in Fig. 1. While recognizing these limitations of our spectra as presented, we are unable to correct all of these differences of level in a rigorous quantitative way because of the limited information available.

Our most complete spectrum (0.8–2.5  $\mu\text{m}$ ) was obtained with SpeX, and because all spectral segments were recorded simultaneously, we use these data as the “backbone” for

Table 1  
Circumstances of observations

Satellite	Date	$\lambda$ region <sup>a</sup>	P.A. ( $\theta$ ) ( $^\circ$ ) <sup>b</sup>	$\alpha$ ( $^\circ$ ) <sup>c</sup>	Lead/trailing
Mimas <sup>d</sup>	2001 Oct. 17	IJHK	268	4.8	Trailing
Mimas <sup>d</sup>	2003 Apr. 7	IJHK	104	5.8	Leading
Enceladus	1995 Sept. 7	K	275	0.9	Trailing
Enceladus	1995 Sept. 9	H	95	0.7	Leading
Enceladus	1998 Oct. 28	K	267	0.6	Trailing
Enceladus	1998 Oct. 28	HK	266	0.6	Trailing
Enceladus <sup>d</sup>	2003 Apr. 5	IJHK	237	5.9	Intermediate
Tethys	1995 Sept. 9	H	265	0.7	Trailing
Tethys	1998 Oct. 28	K	252	0.6	Trailing
Tethys	1998 Oct. 28	HI	249	0.6	Intermediate
Tethys	1998 Oct. 28	KL	236	0.6	Intermediate
Tethys	1998 Oct. 29	JH	55	0.7	Intermediate
Tethys	1998 Oct. 29	J	343	0.7	Intermediate
Dione	1995 Sept. 7	HK	274	0.9	Trailing
Dione	1995 Sept. 9	H	95	0.7	Leading
Dione	1998 Oct. 28	KL	288	0.6	Trailing
Dione	1998 Oct. 28	L	282	0.6	Trailing
Dione	1998 Oct. 29	JH	236	0.7	Intermediate
Dione	1998 Oct. 29	JH	224	0.7	Intermediate
Dione	1998 Oct. 29	J	169	0.7	Intermediate
Rhea	1995 Sept. 7	HK	97	0.9	Leading
Rhea	1995 Sept. 9	H	276	0.7	Trailing
Rhea	1998 Oct. 28	KL	97	0.6	Leading
Rhea	1998 Oct. 28	L	94	0.6	Leading
Rhea	1998 Oct. 29	JH	63	0.7	Intermediate
Rhea	1998 Oct. 29	J	53	0.7	Intermediate
Rhea <sup>d</sup>	2000 Oct. 6	IJHK	110	4.6	Leading
Hyperion	1994 Oct. 6	K	99	3.4	–
Hyperion	1995 Sept. 5	K	274	1.1	–
Hyperion	1995 Sept. 9	H	93	0.7	–
Hyperion	1998 Oct. 29	JH	255	0.7	–
Hyperion	1998 Oct. 29	J	254	0.7	–
Phoebe	1995 Sept. 7	K	58	0.9	–
Phoebe	1995 Sept. 9	H	58	0.7	–

<sup>a</sup> The notation for the wavelength regions covered in various segments of the spectra recorded is that of the standard infrared filter bands, for which the central wavelengths are, respectively, I = 0.88  $\mu\text{m}$ , J = 1.22  $\mu\text{m}$ , H = 1.66  $\mu\text{m}$ , K = 2.18  $\mu\text{m}$ , L = 3.55  $\mu\text{m}$  (Tokunaga, 2000).

<sup>b</sup> P.A. is the position angle of the satellite in its orbit; for synchronously rotating satellites this is a measure of the longitude visible from Earth. For P.A. (longitudes) in the range 70–110 $^\circ$  we were seeing the leading hemisphere of the satellite (in the sense of the orbital motion around Saturn), and for P.A. in the range 250–290 $^\circ$  we were viewing the trailing hemisphere. Hyperion and Phoebe are non-synchronous.

<sup>c</sup>  $\alpha$  is the solar phase angle of the Saturn system, the angle between the Sun and Earth as seen from Saturn.

<sup>d</sup> Observations with the NASA Infrared Telescope Facility (IRTF), SpeX echelle spectrograph.

matching up separate segments of the UKIRT data. In a spectral region of overlap at 2.4  $\mu\text{m}$ , we combine the SpeX data with the long-wavelength UKIRT data to cover the region 0.8–3.6  $\mu\text{m}$ . Shorter wavelength data come from Noll et al. (1997), Voyager photometry (Buratti et al., 1990, and Fig. 2 of Buratti et al., 1998), and Clark et al. (1984). We note the discrepancy between the spectrophotometric data and the shortest Voyager wavelength point (0.33  $\mu\text{m}$ ), and we assign greater weight to the spectrophotometry. The error estimate for the Voyager photometry is  $\pm 0.08$  in geometric albedo

(Buratti et al., 1998). Figure 1 shows all of these segments from 0.22 to 3.6  $\mu\text{m}$ , with the albedo level of each segment scaled to the best of our ability, as described in Appendix A. Discrepancies remain in the absolute levels of several of the segments and even in the slopes of some of the segments, forcing us to make some judgments in the selection of the components to fuse into a final spectrum suitable for modeling.

In terms of the short wavelength region, we see a discrepancy between the shortest wavelength Voyager photometric point (from Buratti et al., 1998) and the ultraviolet spectrum from Noll et al. (1997). The Noll et al. spectrum is plotted with the geometric albedos scale derived in their 1997 paper, which in turn is taken from Roush et al. (1995, Fig. 4) who used a variety of data sources. We retained the albedo scale from the original Noll et al. (1997) paper for the UV segment of the spectrum.

Throughout the rest of the spectrum, we selected segments with the minimum noise, the best overlap, the longest uninterrupted expanses, and best mutual photometric agreement, using our collective scientific judgment. The resulting composite spectrum is shown in Fig. 2, for which the models described below are calculated.

Clark et al. (1984) measured the 0.6–2.5  $\mu\text{m}$  spectrum of the leading hemisphere of Rhea and concluded on the basis of the H<sub>2</sub>O ice band depths that the ice is nearly pure, with less than  $\sim 1$  weight percent particulate minerals, averaged on a global scale. They also noted that the strengths of the ice bands are greater on the leading hemisphere of the satellite, suggesting that the greater incidence of particle radiation on the trailing hemisphere induces some modification of the surface ice. (Note the discrepancy between the text and the figure captions in Clark et al. (1984) concerning the relative band strengths; in fact the bands are stronger on the leading hemisphere, a result corroborated by Grundy et al. (1999).) In our earlier work (Benedix et al., 1998; Dalle Ore et al., 1999) we reported on Hapke models of Rhea using H<sub>2</sub>O ice and ice tholins. In the present paper we present additional models and more details.

We have modeled the spectrum of Rhea using two different theories for diffuse scattering from airless surfaces, Hapke (1981, 1993) theory and Shkuratov theory (Shkuratov et al., 1999). These two theories differ in various ways, but primarily in the way they formulate the scattering particle asymmetry parameter,  $g$ , which governs the single scattering phase function. This in turn affects the calculated abundances of the individual components in multi-component models needed to match astronomical spectra. Poulet et al. (2002) discussed and compared the two theories, and demonstrated the differences with synthetic spectra of H<sub>2</sub>O ice and Titan tholin.

The composite spectrum of Rhea is shown with our best-fit Hapke model in Fig. 2. Our basic approach to Hapke modeling is described by Roush (1994) and Cruikshank et al. (1998b). The goal is to match not only the spectral shape of the satellite's reflectance spectrum, but also the albedo at

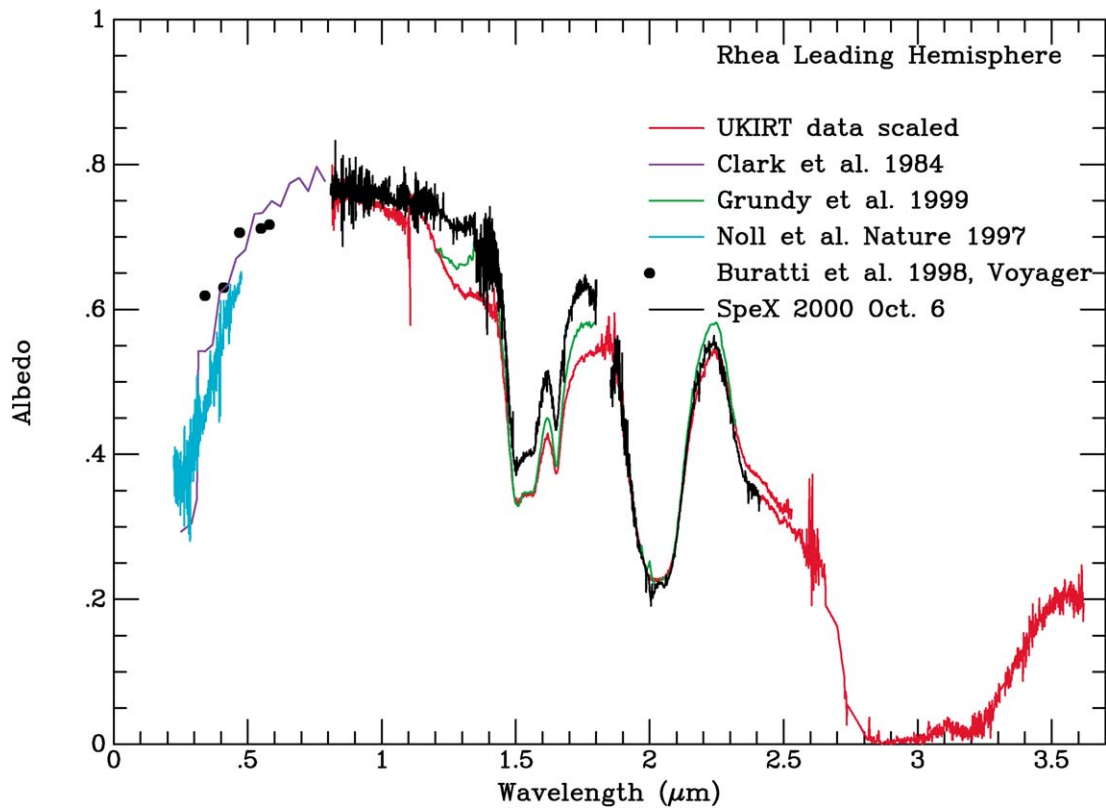


Fig. 1. The spectrum (0.2–3.6  $\mu\text{m}$ ) of the leading hemisphere of Rhea, showing various components from different sources, including the observations discussed in the present paper.

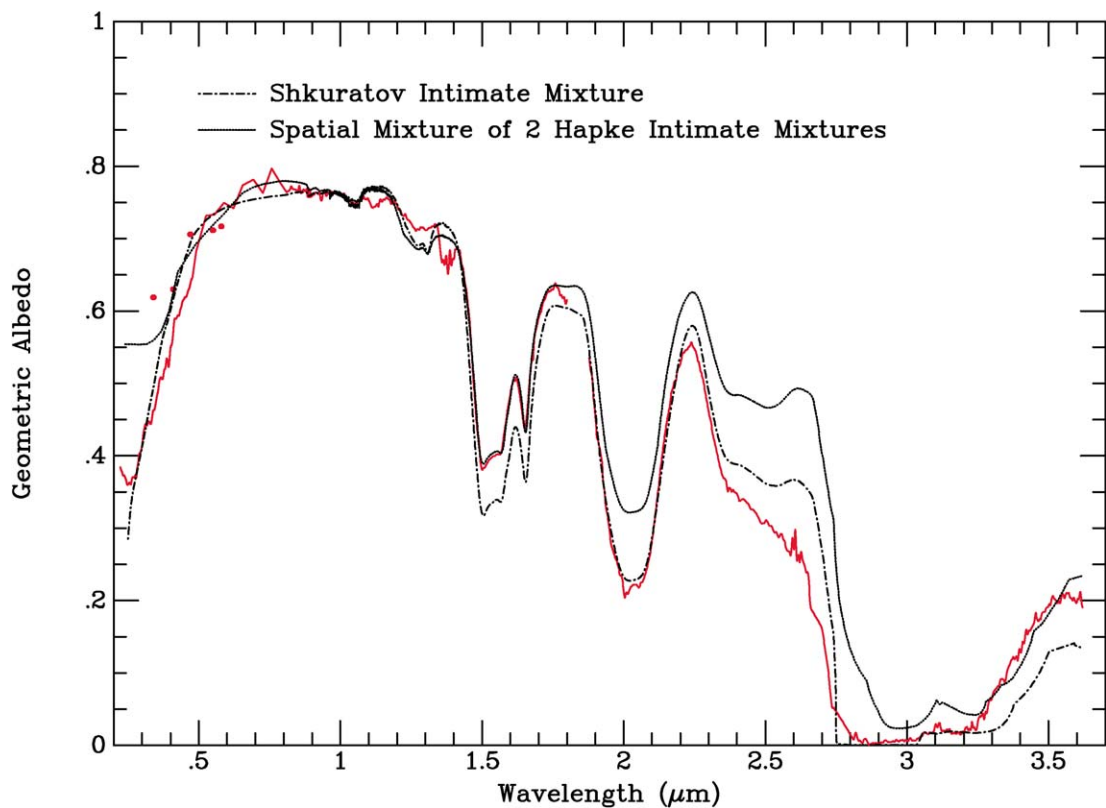


Fig. 2. The composite smoothed spectrum of the leading hemisphere of Rhea (in red) and two models calculated with the Hapke and Shkuratov codes. The minimum in the Rhea spectrum at  $\sim 0.25 \mu\text{m}$  is the  $\text{O}_3$  band reported by Noll et al. (1997);  $\text{O}_3$  is not included in the models.

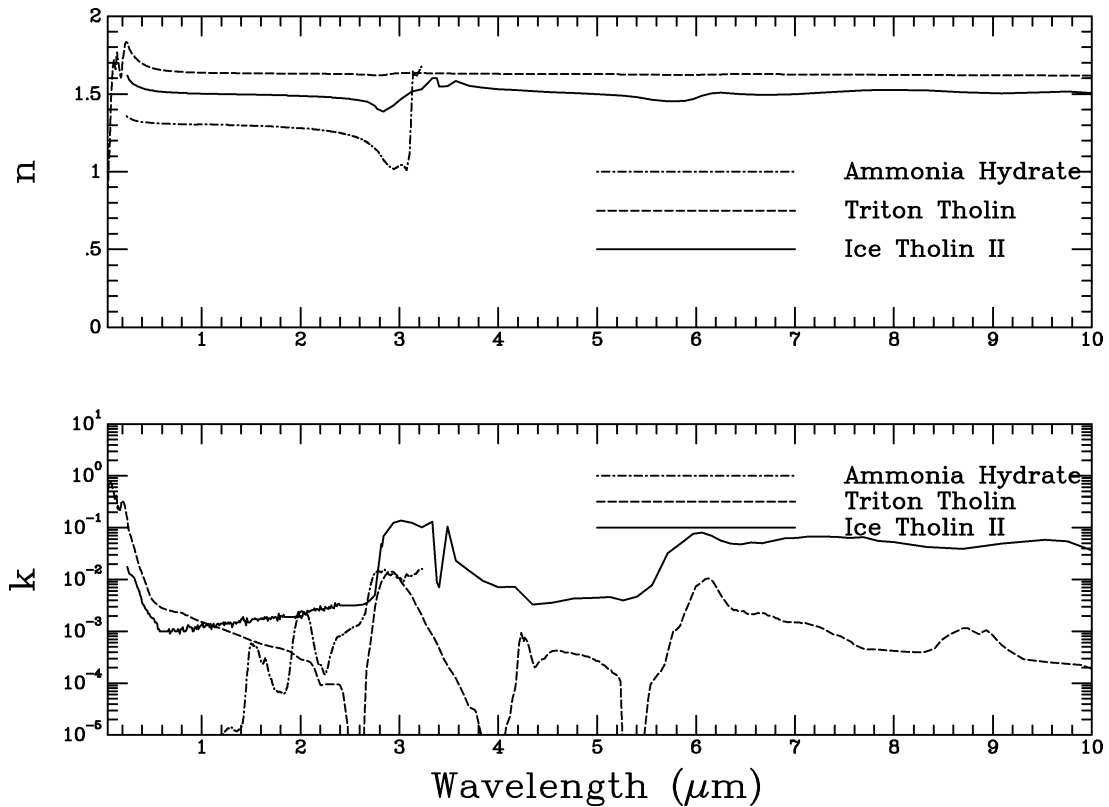


Fig. 3. Complex refractive indices of two components (tholins) of the models for Rhea, provided by Dr. Bishun Khare. Also shown are the complex refractive indices of  $\text{NH}_4\text{OH}$  in  $\text{H}_2\text{O}$ , as noted in text.

every wavelength. Because we are matching the spectrum over a very wide wavelength range (0.22–3.60  $\mu\text{m}$ , a model fit is challenging. Furthermore, we are limited by the number of candidate materials for which reliable optical constants (complex refractive indices) are available. The composite spectrum of Rhea in Fig. 2 is not readily amenable to a calculated formal error at each wavelength point; instead, the uncertainties in the albedo levels and specific spectral features can be judged by the point-to-point scatter in the data and by reference to Fig. 1.

In general terms, continuum albedo between absorption bands is strongly influenced by the scattering coefficients (e.g., Legendre  $b$  coefficient). The strengths of the  $\text{H}_2\text{O}$  ice bands are strongly influenced by particle size, with larger particles giving deeper bands. As grain sizes continue to increase, a distinct blue slope in the overall spectral shape is introduced. Tholins are strongly colored, and mostly affect the short wavelength portion (0.3–1.4  $\mu\text{m}$ ) of the spectrum, where  $\text{H}_2\text{O}$  ice is nearly neutral in reflectance. Certain tholins have a strong N–H absorption band at 3  $\mu\text{m}$ , which appears in the model spectra (note particularly the models of Iapetus in Owen et al., 2001).

After experimenting with many combinations of intimate mixture and spatially segregated models, we converged on the Rhea models shown here (Fig. 2). The Hapke model consists of a spatial mixture of two components, each covering 50% of the leading hemisphere of the satellite. One component consists of an intimate mixture of 95%  $\text{H}_2\text{O}$  ice plus 5%

Ice Tholin II, both in grains 5  $\mu\text{m}$  in size. The second component consists of an intimate mixture of 49.85%  $\text{H}_2\text{O}$  ice (grain size 120  $\mu\text{m}$ ) plus 49.85%  $\text{H}_2\text{O}$  ice (grain size 480  $\mu\text{m}$ ) plus 0.3% Ice Tholin II (grain size 5  $\mu\text{m}$ ). The  $\text{H}_2\text{O}$  ice complex indices were measured at 80 K (Grundy and Schmitt, 1998, and personal communication), and the tholin indices were provided by Dr. B.N. Khare (personal communication, plotted in Fig. 3). Note that in an intimate mixture model an incoming solar photon scatters from grains of all compositional components before emerging.

Additional parameters of our preferred Hapke model are given in Table 2. Whereas a spatial mixture is a simple weighted average of the optical effects of the components, the intimate mixture requires a more complex calculation based on a two-stream approximation to the equation of radiative transfer as developed by Hapke (1993 and references therein). A detailed description of the Hapke equation used here and its parameters is given by Cruikshank et al. (1998b); Eq. (A1) of that paper shows the bidirectional reflectance of a surface and the physical parameters upon which it depends. The parameters we used in the model to calculate the bidirectional reflectance spectrum expressed as geometric albedo are given in Table 2.

As described in Cruikshank et al. (1998b), we assume  $h = 0.05$ ,  $S(0) = 1.0$ , and  $c = 0.0$  for all models, where  $h$  is the compaction parameter,  $S(0)$  is the fraction of light scattered from near the surface at  $g = 0$ , and  $c$  is one of the Legendre polynomial coefficients. The other Legendre

Table 2  
Hapke parameters for the Rhea model

Model components <sup>a</sup>	Materials	Mass fraction	Density (g cm <sup>-3</sup> )	Grain size (mm)	Legendre <i>b</i>
1 A	H <sub>2</sub> O ice	0.9500	0.918	0.005	1.50
1 B	Ice Tholin II in H <sub>2</sub> O ice	0.0500	1.400	0.005	1.50
2 A	H <sub>2</sub> O ice	0.4985	0.918	0.120	1.00
2 B	H <sub>2</sub> O ice	0.4985	0.918	0.480	1.00
2 C	Ice Tholin II in H <sub>2</sub> O ice	0.0030	1.400	0.005	1.00

<sup>a</sup> The preferred model consists of 50% spatial coverage of components 1 and 2, each of which is an intimate mixture of the subcomponents A + B, and A + B + C, respectively, as described in the text.

coefficient (*b*) is varied in this study, and the values used are shown in Table 2 for the different model components. As shown in Eq. (A1) of Cruikshank et al. (1998b),  $\bar{\Theta}$ , the parameter describing the average topographic slope angle of surface roughness at sub-spatial resolution scale, is not used in our calculations; its value is known only at visual wavelengths from the literature and because of our observing conditions it cannot be derived from the observational data.

Our preferred Hapke model matches the 0.5–1.1  $\mu\text{m}$  region reasonably well. The shape of the violet absorption is generally difficult to match, and in our models is entirely attributed to the contribution of the tholin material, which is highly absorbing in the violet and ultraviolet regions. We experimented with all five of the solid organic materials for which complex refractive indices are available to us (see below), and Ice Tholin II yields the best match to the shape. We note, however, that the use of 5- $\mu\text{m}$  grains of the tholin violates the Hapke geometric optics model constraints, at least in the spectral region beyond 3  $\mu\text{m}$  (see below); larger grains worsen the fit at these longer wavelengths by strengthening the absorption of H<sub>2</sub>O ice and lowering the model reflectance at 3.4–3.5  $\mu\text{m}$ .<sup>1</sup>

The H<sub>2</sub>O ice band at 1.6  $\mu\text{m}$  is well fit by the Hapke model, and the temperature-sensitive 1.65- $\mu\text{m}$  band is well matched with the 80 K ice used in the calculations, consistent with Grundy et al. (1999), who found  $T = 81.6 \pm 3.6$  K with their spectrum matching technique (and the same H<sub>2</sub>O ice laboratory data). Neither the 1.3- nor the 2- $\mu\text{m}$  ice band is well fit by our model, and the entire region between 1.9 and 3  $\mu\text{m}$  departs significantly from the Rhea spectrum. We attribute this poor fit to the model parameters and/or the H<sub>2</sub>O ice optical constants, as the spectral data for Rhea appear to be satisfactory in view of the good mutual agreement of the Grundy et al., the SpeX 2000, and the UKIRT data shown in Fig. 1. We further note that the region 2.2–2.5  $\mu\text{m}$  is char-

acteristically difficult to fit with Hapke models and available optical constants, especially for relatively high-albedo surfaces.

The best-fit Shkuratov model, also shown in Fig. 2, consists of an intimate mixture of three components. Component 1 consists of crystalline H<sub>2</sub>O ice (grain size 10  $\mu\text{m}$ ) containing fine absorbing inclusions of Triton tholin in the amount of 0.23%. Component 2 is H<sub>2</sub>O ice (grain size 500  $\mu\text{m}$ ) with inclusions of 0.23% of Triton tholin, and Component 3 is amorphous carbon (grain size > 10  $\mu\text{m}$ ). The components are mixed (at the molecular level) in the proportions 93.3%:6.0%:0.7%. A very similar fit is obtained with an intimate mixture of Component 1 = H<sub>2</sub>O (10  $\mu\text{m}$  grains) with 0.049% Titan tholin, Component 2 = H<sub>2</sub>O (380  $\mu\text{m}$  grains) with 0.049% Titan tholin, and Component 3 = amorphous carbon (size > 10  $\mu\text{m}$ ), mixed in the proportions 92.4%:6.8%:0.8%. The tholin inclusions can be distributed throughout the H<sub>2</sub>O ice particle or near the surface. This kind of mixing is called intraparticle or molecular mixing (Poulet et al., 2002) in which the complex refractive indices of the mixture are calculated by effective medium theory (e.g., Bohren and Huffman, 1983; Wilson et al., 1994; Cuzzi and Estrada, 1998; see also Cruikshank et al., 2003). In the Shkuratov modeling we used  $g = 0.6$ , in accordance with the approximate calculated value for ice particles shown in Poulet et al. (2002, Fig. 3), and the Rhea spectrum was fit using a simplex technique and 325 points uniformly spaced throughout the spectrum.

Our models do not give uniquely good fits to the data; other scattering parameters, other non-ice components, and other scattering theories might give improved fits. Also, the number of significant figures in some of the modeling parameters suggests a degree of sensitivity of the fits to the data that is perhaps misleading. While the quality of fit of the preferred models is in fact sensitive to these parameters at a high level of accuracy, the models themselves have many more physical parameters that are not well known for most bodies in the Solar System. In addition, the complex refractive indices of the materials we use in the models are in some cases uncertain by 30% or more. Once a set of refractive indices is selected and other parameters of particle scattering are chosen, the calculated models are quite sensitive to the abundances of the components, their grain sizes, and their mixing geometry. Furthermore, in evaluating the “quality of fit” of a model to the data, a standard chi-squared technique is used, tempered with visual inspection that accounts for variations in the quality of the observational data in different wavelength regions, and other uncertainties in aspects of the quality of the data that do not translate numerically to the chi-squared analysis.

The Shkuratov model fits the spectral region 0.3–1.4  $\mu\text{m}$  very well, and reproduces the shape and level of the 2- $\mu\text{m}$  ice band satisfactorily, although the 1.55- $\mu\text{m}$  ice band is too deep in the model. The strong H<sub>2</sub>O ice band at 3  $\mu\text{m}$  is fit only approximately.

<sup>1</sup> Piatek (2002, 2003) find that the scattering properties of small particles disagree strongly with predictions that they act as independent particles with dominantly forward scattering. Thus, for reasons not yet understood, the use of particles of size comparable to the wavelength of the light in Hapke theory does not invalidate the results.

As in the case of the Hapke models, decreasing the grain size improves the fit beyond 3  $\mu\text{m}$ , but similarly violates the geometric optics constraints of the Shkuratov model. We also found in several tests that pure water ice mixed with tholins intimately or spatially does not yield a satisfactory fit to the spectrum. The importance of the intra- or molecular mixing of water ice and tholin (as noted above) in the Shkuratov models is thus corroborated (see Poulet et al., 2002).

Because we have been unable to find a fully satisfactory model using either the Hapke or Shkuratov codes, and because each of our best-fit models fails in the region  $\sim 2.3\text{--}2.9 \mu\text{m}$ , we explore the possibility that an additional absorbing species might be present on Rhea. We note that this spectral region has been particularly difficult to fit in other modeling attempts for other objects (e.g., Calvin and Clark, 1991; Davies et al., 1997; Buie and Grundy, 2000). Owen et al. (2001) succeeded with the Hapke code in fitting the low-albedo hemisphere of Iapetus, but it was necessary to violate the small-particle limit in the Hapke theory. In Fig. 4 we show the ratio of data to the best-fitting Hapke and Shkuratov models (data/model), revealing the characteristics of the lack-of-fit. In some regions of the spectrum (1.12–1.15, 1.35–1.40, 1.82–1.90, and 2.5–2.6  $\mu\text{m}$ ) discrepancies can be attributed to incomplete cancellation of telluric absorption bands.

Grundy and Schmitt (1998) estimate that the error in the absolute absorption coefficient in  $\text{H}_2\text{O}$  ice in the region of strong absorptions is several percent, while in regions of weak absorption the uncertainty could be a factor of  $\sim 2$ . We find the greatest discrepancy between the models and Rhea in the region of the strongest absorption band ( $\sim 2.7\text{--}3.4 \mu\text{m}$ ) in the wavelength interval we cover. Absorption in this and the other strong  $\text{H}_2\text{O}$  ice bands is strongly dependent on particle size (e.g., Calvin and Clark, 1991, Fig. 5), and a perfectly fitting model may require many different particle sizes in a variety of microphysical settings and ice grain configurations. Absorption attributed to  $\text{H}_2\text{O}_2$  at  $\sim 3.4 \mu\text{m}$  has been reported in the spectrum of Europa (Carlson et al., 1999). Small amounts of this molecule may

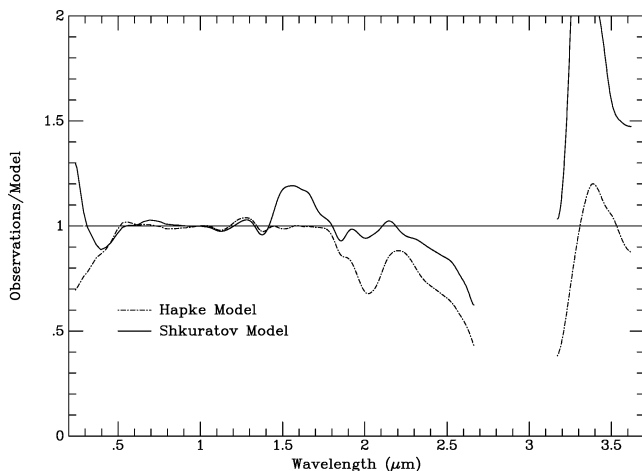


Fig. 4. Smoothed ratio of Rhea spectral data to the models in Fig. 2.

be produced in the  $\text{H}_2\text{O}$  ice by irradiation. A quantitative evaluation of possible  $\text{H}_2\text{O}_2$  absorption on Rhea and the other satellites of Saturn awaits the Cassini mission and the acquisition of spatially resolved spectra of high signal precision.

It does not seem that the imperfect fits arise from incorrect absorption coefficients in  $\text{H}_2\text{O}$  ice. The discrepancy between the models and the spectrum of Rhea might be interpreted as a broad absorption band characteristic of organic solids different from the tholin we used in the model. Inspection of the reflectance spectra of four tholins in Fig. 2 of Cruikshank et al. (1991) shows that none of these materials satisfies the condition that the reflectance must rise rapidly longward of  $\sim 3.2 \mu\text{m}$ , and there are other discrepancies as well. Among several minerals examined in the U.S. Geological Survey on-line spectral database (Clark et al., 1993), kaolinite (aluminum-bearing clay) and beryl (beryllium aluminum silicate) have absorption bands with approximately the correct shape between 2.3 and 3  $\mu\text{m}$ . We do not pursue this matter further here because of the weak foundation for the existence of such a band on Rhea. Silicate minerals normally present strong  $\text{Fe}^{2+}$  and  $\text{Fe}^{3+}$  absorptions in the 0.9–1.1  $\mu\text{m}$  region, but we see no evidence for these in any of the satellite spectra.

While we might speculate that the misfit of the model could arise from the effects of a multiplicity of  $\text{H}_2\text{O}$  ice particle sizes and shapes on Rhea, or the presence of yet unidentified additional absorbers, we leave the matter unresolved at this time. When spectra of Rhea and the other satellites with high spatial resolution become available from the Visual-Infrared Mapping Spectrometer (VIMS) on the Cassini spacecraft, all the issues connected with modeling will be reopened.

## 2.2. The role of tholin in the models

In both the Hapke and Shkuratov models of Rhea, we included a small quantity of tholin with the  $\text{H}_2\text{O}$  ice; as noted above, it was included as an inclusion in the ice in the Shkuratov models. The role of the tholins is two-fold. First, they provide the absorption in the spectrum that begins at about 0.7  $\mu\text{m}$  and increases toward the ultraviolet. The spectrum of Rhea in this region has a curved shape that is not matched by any of the other materials that we tried in our models; those materials included the igneous minerals olivine and pyroxene, HCN polymer, and the meteorites Allende and Murchison. In models of the low-albedo hemisphere of Iapetus, Owen et al. (2001) found that a tholin was needed to provide the strong red color in the spectral region shortward of 1  $\mu\text{m}$ , and in models of the very red colored surface of Centaur objects 5145 Pholus, Cruikshank et al. (1998c) found that a tholin was required to fit the same spectral region.

Second, tholins have relatively high reflectance longward of  $\sim 3.2 \mu\text{m}$ , and they therefore quench the very strong absorption of  $\text{H}_2\text{O}$  ice in this spectral region. This effect of

Table 3  
Tholins

Name	Starting mixture	Energy source	References
Triton tholin	Gaseous N <sub>2</sub> :CH <sub>4</sub> (99.9:0.1)	Plasma discharge	McDonald et al. (1994)
Titan tholin	Gaseous N <sub>2</sub> :CH <sub>4</sub> (9:1)	Plasma discharge	Khare et al. (1984), McDonald et al. (1994)
Ice Tholin I	H <sub>2</sub> O:C <sub>2</sub> H <sub>6</sub> (6:1)	Plasma discharge	Khare et al. (1993), McDonald et al. (1996)
Ice Tholin II	H <sub>2</sub> O:CH <sub>3</sub> OH:CO <sub>2</sub> :C <sub>2</sub> H <sub>6</sub> (80:16:3.2:0.8)	Plasma discharge	McDonald et al. (1996)

tholin was especially important in the case of the Iapetus study (Owen et al., 2001) because of the narrow character of the strong absorption band centered at 3.0  $\mu\text{m}$  in the satellite's spectrum. The spectrum of Rhea begins to rise in reflectance at 3.2  $\mu\text{m}$ , while that of pure H<sub>2</sub>O ice (seen in reflectance on a surface) continues to absorb strongly at this and longer wavelengths. Thus, the 3- $\mu\text{m}$  region becomes a strong discriminator for the presence of impurities to the basic H<sub>2</sub>O ice, and while the Shkuratov model gives an overall better fit to the Rhea data, the Hapke model fits best in the region that is critical to the tholin properties.

In the Pholus models (Cruikshank et al., 1998c), Titan tholin was included as a distinct particulate component of the intimate mixtures of particles of different composition, but the tholin particle size was smaller than that formally allowed by Hapke theory. Poulet et al. (2002) calculated a Shkuratov model of Pholus in which the tholin was included as a molecular contaminant to the H<sub>2</sub>O ice particles, accomplished by mixing the optical constants of ice and tholin in certain proportions. The version of the Shkuratov code we used correctly accounts for the mixing of optical constants using effective medium theory.<sup>2</sup>

Tholins may also occur in the icy particles of Saturn's ring system. Cuzzi and Estrada (1998) found that the particles in the A and B rings contain a material imparting a red color (absorption toward the violet spectral region), while the particles in the C ring and Cassini's division are lower in albedo and less red in color. They note that, "No silicates have the appropriate combination of steep spectral slope and high absorptivity to explain the rings' visual color while remaining compatible with microwave observations." Titan tholin easily matches the colors and albedos of the particles when incorporated into the scattering models with H<sub>2</sub>O ice. To explain the lower albedo and more neutral color of the darker rings, Cuzzi and Estrada (1998) suggest that "material with properties like carbon black, as seen in at least some comets and interplanetary dust particles, is needed. . . ." Subsequent modeling of the rings by Poulet and Cuzzi (2002)

and Poulet et al. (2003) also incorporated tholins and amorphous carbon to achieve fits to the observational data (0.3–4  $\mu\text{m}$ ).

We experimented with models using four tholins for which optical constants have been determined. These materials, all of which were prepared at Cornell University, are shown in Table 3.

In modeling Rhea's leading hemisphere over the limited spectral range 0.22–0.48  $\mu\text{m}$ , Noll et al. (1997) included Ice Tholin I, which, together with solid ozone, provided the best fit. Ice Tholin I gives a less satisfactory fit than Titan tholin over the much wider spectral range included in this paper. Although Noll et al. (1997) identified solid O<sub>3</sub> in the ultraviolet spectra of Rhea (and Dione), evidenced by an absorption band centered at 0.26  $\mu\text{m}$ , we do not include O<sub>3</sub> in the models presented here, because of a lack of suitable optical constants for this molecule over the spectral range we consider. At the same time, we do not expect trace amounts of O<sub>3</sub> in the H<sub>2</sub>O ice of Rhea (and Dione) to have a significant effect on the appearance of the spectra beyond the ultraviolet, apart from a possible weak band near 0.6  $\mu\text{m}$ , based on the gas phase O<sub>3</sub> spectrum.

Ramirez et al. (2002) have published complex refractive indices (0.2–0.9  $\mu\text{m}$ ) for a new tholin produced by cold plasma discharge in a gas that simulates Titan's atmosphere. The values of the imaginary refractive index,  $k$  in the region of our modeling (0.3–0.9  $\mu\text{m}$ ) are less than those of the Titan tholin of Khare et al. (1984) by a factor ranging from about 5 to 15, and the shape of the absorption spectrum is different. Thus, the use of the Ramirez et al. tholin in our models would require more material to achieve the same degree of absorption. More importantly, the shape of the model output does not fit well when this tholin is used. Other tholins are becoming available as additional experimentation continues in an effort to understand Titan's atmosphere and aerosols (Imanaka et al., 2004). This expansion of the library of optical constants will assist with future modeling of solid surfaces. Tran et al. (2003) have published spectra of their Titan tholin for  $\lambda > 2.5 \mu\text{m}$ ; optical constants are not yet available.

We emphasize that the tholins in our model are considered *representative* of a very broad class of complex organic solids produced by energy deposition in gases and ices having compositions of planetary relevance. Although we have achieved a reasonable model fit with specific tholins in the region where those materials absorb most strongly, we do not assert that these *specific* materials are present on Rhea and the other icy satellites.

<sup>2</sup> Effective medium theory allows an estimate of the complex refractive indices of a combination of materials when one component is present as microscopic inclusions in a host material. The optical properties of such an inhomogeneous medium are described by a complex dielectric function and a complex magnetic permeability. The Maxwell Garnett approximation can be used for two-component mixtures in which the host material is isotropic and the inclusions are either isotropic or anisotropic (Levy and Stroud, 1997). Shkuratov et al. (1999, Eqs. (15)–(18)) show the formulation for coarse particles with fine absorbing independent inclusions.

### 2.3. Search for other absorbing species

The high quality and spectral resolution of the spectra presented here allow us to make meaningful searches for additional absorbing species among the several ices that have been observed in the laboratory under conditions relevant to the satellites of the outer planets (e.g., Bohn et al., 1994; Schmitt et al., 1998). The fact that ices occur in various complex combinations is clear from the cases of Triton, where five different ices are found (Cruikshank et al., 1993, 2000; Quirico et al., 1999), and Pluto, where four different ices are seen (Owen et al., 1993; Douté et al., 1999). We have searched our spectra of Rhea and the other large saturnian satellites for species other than H<sub>2</sub>O ice, with the results given below. We emphasize that these results pertain to spectra of an entire hemisphere of a given satellite, and that future spectra of regions on these bodies at a smaller spatial scale may reveal absorbing species that cannot be seen at hemispheric scales because of spectral dilution, as in the case of the satellites of Jupiter (e.g., McCord et al., 1998). Furthermore, the detection sensitivity depends upon several factors, including the nature of the mixing with other components, particle size, scattering phase functions, etc.

To search for other constituents in the spectra, we calculated synthetic spectra using the Hapke code and optical constants for the relevant materials. The upper limits we derive are dependent to varying degrees on the modeling code used, and we cite the example of the comparison of Hapke and Shkuratov models of Centaur 5145 Pholus presented in Poulet et al. (2002). The two codes give considerably different abundances of the same components in models of the Pholus spectrum having comparable goodness of fit. For consistency, we use a single code (Hapke) in modeling the upper limits presented here.

#### 2.3.1. CO<sub>2</sub>

To search for the three narrow bands of CO<sub>2</sub> ice at 1.97, 2.01, and 2.06 μm, we calculated synthetic spectra at the resolution of our satellite data, using a basic H<sub>2</sub>O ice intimate mixture Hapke scattering model. We then added CO<sub>2</sub> in various amounts and grain sizes to establish the strength of the bands and estimate the minimum amount that could be detected at the level of signal precision of our data for Rhea and the other satellites. Figure 5 shows a model with 25% CO<sub>2</sub> and three different grain sizes, with the spectrum of Rhea for comparison. From intimate mixture models, the upper limit for CO<sub>2</sub> on Rhea for 5 μm grains is ~2 weight percent, for 50 μm grains ~5 weight percent, and for 500 μm grains ~20 weight percent.

#### 2.3.2. CH<sub>4</sub>

The spectrum of methane ice is rich with strong absorption bands in the K-region. We have used these bands to set an upper limit to the amount of methane ice by progressively adding CH<sub>4</sub> to a Hapke model that otherwise matches the H<sub>2</sub>O absorption spectrum of Rhea. Figure 6 shows three dif-

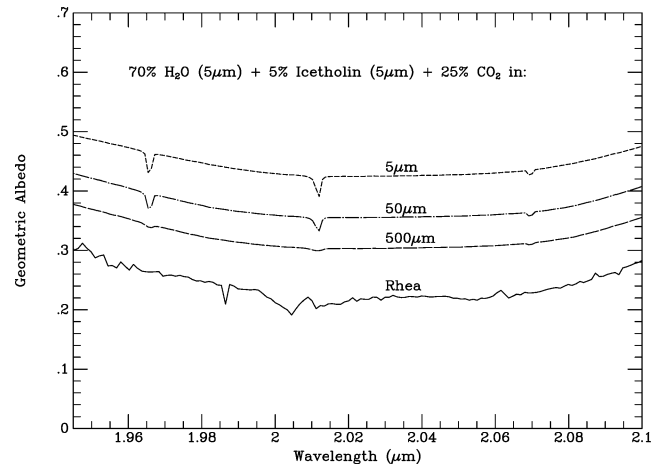


Fig. 5. A segment of the spectrum of Rhea (bottom trace), and three model spectra with 25% CO<sub>2</sub> ice in three different grain sizes, intimately mixed with H<sub>2</sub>O ice. The increasing albedo with decreasing particle size is correctly shown in this graph. The CO<sub>2</sub> bands occur at 1.966, 2.012, and 2.070 μm.

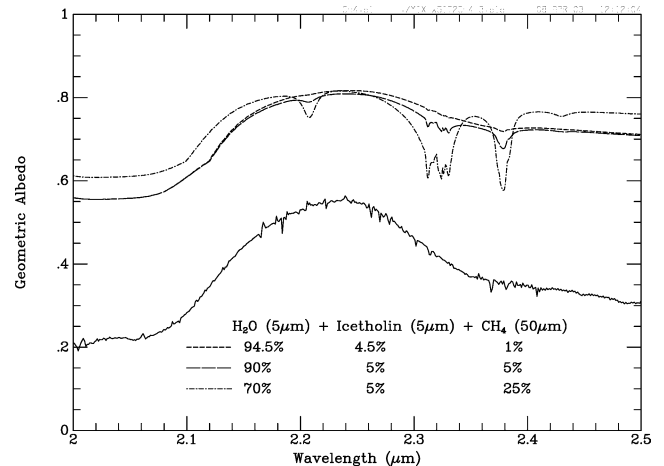


Fig. 6. A segment of the spectrum of Rhea (bottom trace), and three model spectra with different amounts of CH<sub>4</sub> ice mixed with H<sub>2</sub>O ice. The traces with CH<sub>4</sub> absorption bands are vertically offset from the Rhea spectrum. The principal CH<sub>4</sub> absorption bands occur at 2.21, 2.32, and 2.38 μm.

ferent amounts of CH<sub>4</sub> ice in the model, and the spectrum of Rhea. From intimate mixture models, the upper limit for CH<sub>4</sub> ice on Rhea for both 5 and 50 μm grains is ~2 weight percent.

#### 2.3.3. NH<sub>3</sub> and ammonium compounds

The presence on any of Saturn's satellites of ammonia as a pure ice, as a hydrate with H<sub>2</sub>O ice, or as frozen NH<sub>4</sub>OH, would be of special interest, primarily because ammonia depresses the freezing temperature of H<sub>2</sub>O. Brown and Calvin (2000), for example, have reported a possible detection of ammonia ice (NH<sub>3</sub> or NH<sub>3</sub>•2H<sub>2</sub>O) on Charon to account for an absorption band at 2.2 μm. Bauer et al. (2002) suggest that NH<sub>3</sub>•H<sub>2</sub>O might give rise to a feature at ~2.2 μm in the spectrum of the uranian satellite Miranda. Because images of some of Saturn's satellites show surface regions suggestive

Table 4  
Absorption bands of ammonia ice, ammonium hydroxide, and ammonia hydrate

	Wavelength $\mu\text{m}$	Frequency $\text{cm}^{-1}$	Absorption coefficient $\text{cm}^{-1}$
NH <sub>3</sub> ice <sup>a</sup>	2.005	4988	450
	2.237	4470	910
	2.247	4450	390
	2.964	3374	45000
	2.962	3368	22000
	2.970	3367	27000
	3.101	3225	800
NH <sub>3</sub> hydrate <sup>b</sup>	1.983	5044	120
	1.994	5014	215
	2.209	4526	80
	2.220	4505	95
NH <sub>3</sub> hydrate <sup>c</sup>	2.950	3390	Not available
	3.001	3332	“
	3.032	3298	“
	3.115	3210	“
	3.431	2915	“
	NH <sub>3</sub> hydrate <sup>d</sup>	1.993	5107
2.210		4524	“
NH <sub>4</sub> OH <sup>e</sup>	1.04	9615	“
	1.22	8197	“
	1.30	7692	“
	1.53	6536	“
	1.63	6135	“
	1.99	5025	“
	2.21	4525	“

<sup>a</sup> Sill et al. (1980). <sup>b</sup> Schmitt et al. (1998). <sup>c</sup> Sill et al. (1981).  
<sup>d</sup> S. Sandford (this paper). <sup>e</sup> Brown et al. (1988).

of the relatively recent flow of fluids, the issue of materials and sources arises. We have given particular attention to the detection of solid NH<sub>3</sub>, NH<sub>3</sub> hydrate, and NH<sub>4</sub>OH on the satellites because they have distinguishing absorption bands in the spectral region covered by our data.

We prepared an ammonia hydrate ice by co-depositing H<sub>2</sub>O and NH<sub>3</sub> in various relative concentrations at 10, 70, and 90 K, and then warming the ice film to various temperatures up to 150 K. The most prominent and useful absorption bands were found in transmission spectra of thin films at 1.993 and 2.210  $\mu\text{m}$ . Bands at the same wavelengths were also seen in an ammonia hydrate examined by Schmitt et al. (1998); they are clearly different in wavelength from pure NH<sub>3</sub> bands (e.g., Slobodkin et al., 1978; Sill et al., 1980, 1981; Schmitt et al., 1998). In reflectance spectra of granulated, frozen NH<sub>4</sub>OH, Brown et al. (1988) found several absorption bands, including those at 1.99 and 2.21  $\mu\text{m}$  (the spectra were relatively low resolution, and the wavelengths could not be determined with any greater precision than three significant figures). Table 4 summarizes the available information on ammonia ices in the wavelength region of relevance in the present work.

Figure 7 presents the 1.3–2.4  $\mu\text{m}$  spectrum of Rhea and three Hapke models in which the optical constants of NH<sub>4</sub>OH ice (1% NH<sub>4</sub>OH in H<sub>2</sub>O) have been substituted for

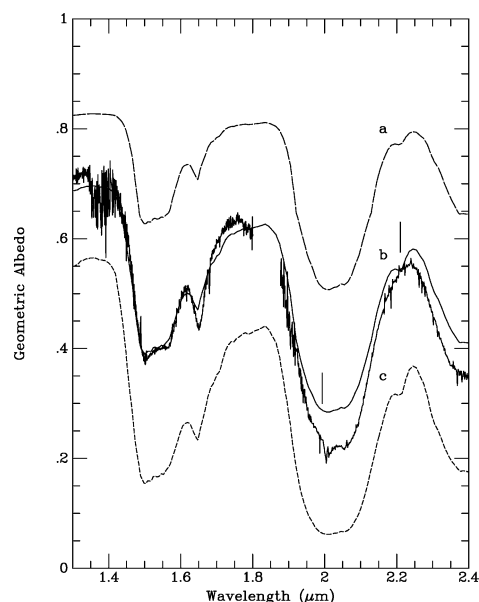


Fig. 7. A section of the spectrum of Rhea and a model calculated with NH<sub>4</sub>OH (1 percent solution) ice instead of H<sub>2</sub>O ice. Vertical lines at 1.99 and 2.21  $\mu\text{m}$  indicate the positions of the two principal absorptions of NH<sub>4</sub>OH. Model *a* is an intimate mixture of 95% NH<sub>4</sub>OH + 5% Ice Tholin II, all in 5  $\mu\text{m}$  grains. Model *c* is an intimate mixture of 49.85% NH<sub>4</sub>OH (120  $\mu\text{m}$  grains) + 49.85% NH<sub>4</sub>OH (480  $\mu\text{m}$  grains) + 0.3% Ice Tholin II (5  $\mu\text{m}$  grains). Model *b*, which gives a good overall fit to the Rhea spectrum, but shows the additional feature (2.21  $\mu\text{m}$ ) not present on Rhea, is a spatial mixture of 50% each of models *a* and *c*.

those of pure H<sub>2</sub>O ice. The optical constants (Fig. 3) for the NH<sub>4</sub>OH ice were derived (by T. Roush) from laboratory reflectance spectra published by Brown et al. (1988). The first step of the procedure was to estimate the sample particle size from the lab spectra by matching the depths and shapes of the measured H<sub>2</sub>O bands with Hapke models of pure ice (80 K). With a value for the characteristic particle size, the values of the refractive indices  $n$  and  $k$  across the spectrum were then calculated using Hapke theory, as described by Clark and Roush (1984) and Lucey (1998).

There is no evidence for any absorption bands in the spectrum of Rhea or the other satellites attributable to ammonia in any of its forms. We estimate that the 2.21- $\mu\text{m}$  band would be visible in the presence of  $\geq 0.5$  weight percent NH<sub>3</sub> in water ice as a hydrate or as frozen NH<sub>4</sub>OH on any of the satellites.

#### 2.3.4. Other molecules

The magnetosphere of Saturn contains plasma ions that impact the rings and satellites, carrying the potential to cause chemical changes in their surface materials. Ions of N<sup>+</sup> and N<sub>2</sub><sup>+</sup> originating from Titan and implanted into the surface ices of the large satellites should induce chemical changes resulting in many combinations of N, H, and O (Delitsky and Lane, 2002). With the list of expected species from Delitsky and Lane, plus the spectra of various ices presented by Quirico and Schmitt (1997), we have searched for various possible constituents of the surface of Rhea. From a qualita-

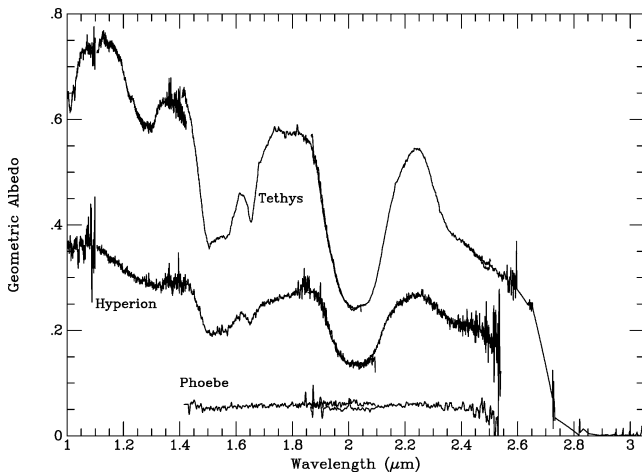


Fig. 8. Spectra of Tethys, Hyperion, and Phoebe, using UKIRT CGS4 data for 1994–1998 (Table 1). The data for Tethys extend to 3.05  $\mu\text{m}$ , while the others terminate at 2.55  $\mu\text{m}$ . The Phoebe spectrum has been described and modeled by Owen et al. (1999), and is included here to show its contrast to the spectra of the other objects.

tive comparison of the published spectra we find no evidence for any spectral features that might indicate the presence of  $\text{SO}_2$ ,  $\text{NO}_2$ ,  $\text{HC}_3\text{N}$ ,  $\text{C}_2\text{H}_2$ ,  $\text{C}_2\text{H}_4$ ,  $\text{C}_2\text{H}_6$ , or  $\text{C}_3\text{H}_8$  in our hemispherically averaged spectrum of Rhea or in spectra of the satellites discussed below.

### 3. Other icy satellites

In this section we discuss our near-infrared spectra of several other satellites, but we do not model each one explicitly. These objects vary in geometric albedo from one to the other (e.g., Buratti et al., 1998, Table 3), but their globally averaged, near-infrared spectra are remarkably similar, with some interesting exceptions discussed below. The data presented in Figs. 8 and 9 were obtained with the UKIRT and the CGS4 spectrometer in 1994–1996 when the view of the Saturn system was nearly in Saturn's equatorial plane. Each spectrum has been assembled from two or three wavelength segments observed separately (see Table 1), and scaled to the correct geometric albedo using photometry in the H and K bands (Appendix A). When viewed in this way, differences and similarities among the spectra become apparent.

All of the satellite spectra in Figs. 8 and 9 show the characteristic absorption bands of  $\text{H}_2\text{O}$  ice at 1.5, 1.65, 2.0, and 2.5  $\mu\text{m}$  (and some show the 1.25- $\mu\text{m}$  band), although there are differences from object to object that merit notice and comment. In some of the spectra there is residual noise around 1.88  $\mu\text{m}$  due to incomplete cancellation of the effects of telluric atmospheric  $\text{H}_2\text{O}$  vapor. Associated with the incomplete cancellation, anomalous slopes in adjacent wavelength regions may have been introduced into the reduced spectra, a point to which we return below. The symmetrical absorption centered at 1.65  $\mu\text{m}$  seen in the spectra of all the satellites is particularly diagnostic of the hexag-

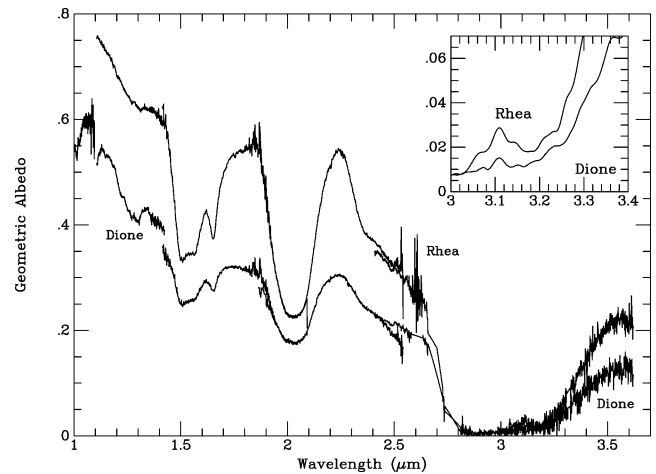


Fig. 9. Spectra of Rhea and Dione, using UKIRT CGS4 data for 1994–1998. The inset shows the region of the Fresnel peak in  $\text{H}_2\text{O}$  ice, smoothed and plotted on an expanded scale. Because of a presumed inaccuracy in the original wavelength scale derived for the Dione observation, the data for this satellite in the inset were offset by +0.017  $\mu\text{m}$  to bring the Fresnel peak into agreement with its correct position as shown in the Rhea spectrum.

onal phase of  $\text{H}_2\text{O}$  ice, as well as the temperature of the ice (Fink and Larson, 1975; Grundy and Schmitt, 1998; Grundy et al., 1999).

We note that there is no indication of the 1.85  $\mu\text{m}$  absorption reported by Clark et al. (1984) in the trailing hemisphere of Tethys, and weakly visible in the spectra of the leading hemisphere of Rhea and Dione published by those authors. This feature may have been caused by incomplete cancellation of telluric absorptions, as Clark et al. (1984) anticipated.

Figure 9 shows the 3- $\mu\text{m}$  region of the spectra of Rhea and Dione, with the Fresnel peak enlarged and smoothed for comparison. The weaker Fresnel peak on Dione is consistent with the overall lower albedos, which may arise from the presence of material of low albedos mixed with the water ice. Owen et al. (2001) showed that the intimate mixture of greater than about 10% of minerals or other material of low albedos suppresses the strength of the Fresnel peak.

The region 1.9–2.5  $\mu\text{m}$  is shown on an expanded scale in Fig. 10. Many molecules of planetary relevance (see Figs. 4–6; Bohn et al., 1994; Quirico and Schmitt, 1997) have absorption bands in this spectral interval, thus giving it special significance. The quality of the data in Fig. 10 and the lack of discernible absorption bands support our assertion that no ices other than  $\text{H}_2\text{O}$  are visible in the spectra of the five satellites shown.

#### 3.1. Mimas

In Fig. 11 we show two spectra of Mimas obtained with IRTF/SpEX. The spectrum from 2001 shows the trailing hemisphere, while the 2003 spectrum is largely the leading hemisphere. The albedo scale is set at  $0.73 \pm 0.03$  at 0.9  $\mu\text{m}$  from the Buratti et al. (1998) analysis of Voyager photometry of Mimas' trailing hemisphere; the lower trace in Fig. 11 is offset in geometric albedo by  $-0.2$  for clarity. The Buratti

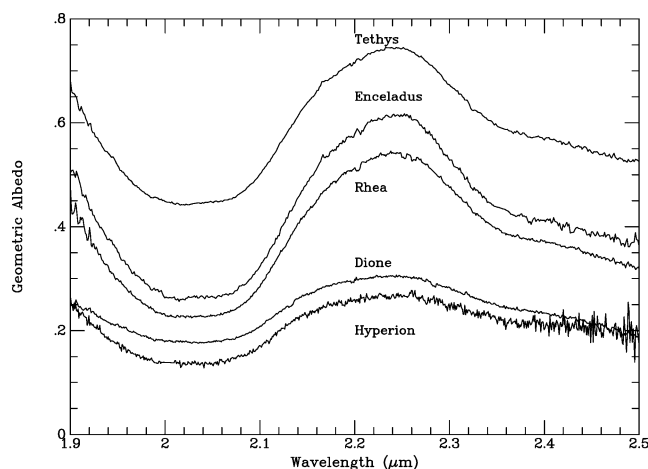


Fig. 10. Spectra of five satellites from 1998 data, 1.9–2.5  $\mu\text{m}$ . The spectrum of Tethys is offset by +0.2 in geometric albedo for clarity. Positions of the potential minor constituents discussed in the text are shown.

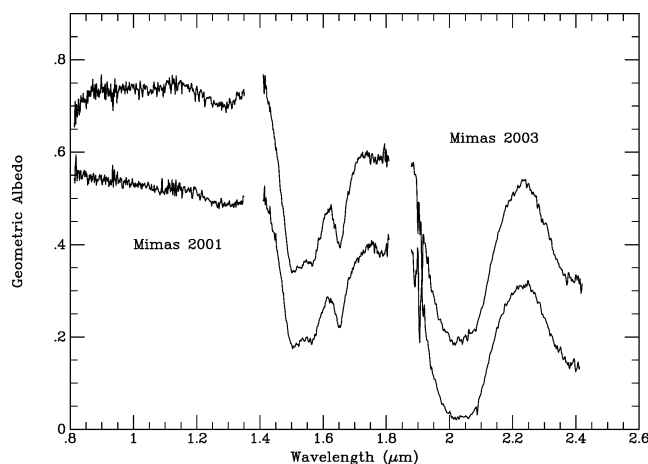


Fig. 11. Two spectra of Mimas with the SpeX spectrometer. The spectrum of October 17, 2001 shows the trailing hemisphere, and that of April 7, 2003 is primarily the leading hemisphere. The geometric albedo scale is set by the Buratti et al. (1998) analysis of Voyager photometry of Mimas' trailing hemisphere; the lower trace is offset by  $-0.2$ .

albedo is consistent with Roddier et al. (2000), who found  $0.78 \pm 0.10$  at J and  $0.55 \pm 0.03$  at H, also for the trailing hemisphere, but not with the value of  $0.66 \pm 0.04$  at K found by Momary et al. (2000). Both spectra clearly show the presence of crystalline  $\text{H}_2\text{O}$  ice, with a prominent  $1.65 \mu\text{m}$  absorption band. The principal differences we see in these two spectra are the continuum shape, the strength of the  $1.3 \mu\text{m}$   $\text{H}_2\text{O}$  ice band, and a possible absorption band at  $1.78 \mu\text{m}$  that is particularly notable in the 2001 spectrum. The greater strengths of the  $\text{H}_2\text{O}$  ice bands on the leading hemisphere are consistent with the observations of Clark et al. (1984) for the other satellites; the weaker bands on the trailing hemisphere may be a consequence of irradiation by charged particles in Saturn's rotating magnetosphere. Similarly, the questionable absorption band at  $1.78 \mu\text{m}$  on the trailing hemisphere might arise from irradiation. On the other hand, this feature lies

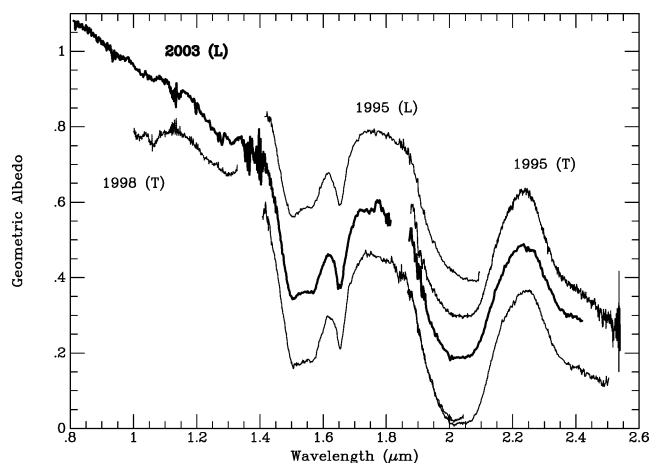


Fig. 12. Spectra of Enceladus. The SpeX data for 2003 are scaled to the Voyager value of the albedo of Enceladus (see text). The 1998 spectrum is offset by  $-0.2$ , and the two spectrum segments obtained in 1995 are offset by  $+0.25$ .

near the region of strong telluric water vapor interference, and may be spurious.

### 3.2. Enceladus

We have observed the spectrum of Enceladus in the region  $0.8$ – $2.55 \mu\text{m}$ , various segments having been recorded at various times with different telescopes between 1995 and 2003. Consistent with the work of other investigators, we have detected no spectral features other than those diagnostic of  $\text{H}_2\text{O}$  ice. The high albedo of Enceladus results in a colder surface than most of the other satellites, with a calculated subsolar temperature of  $75 \pm 3 \text{ K}$ , and an average temperature of  $\sim 51 \text{ K}$ . The  $1.65\text{-}\mu\text{m}$  temperature-sensitive ice band is correspondingly stronger than for most of the other satellites.

Three spectra of Enceladus are shown in Fig. 12. The SpeX spectrum for the leading hemisphere observed in 2003 shows a steep negative continuum slope throughout the range  $0.8$  to  $2.4 \mu\text{m}$ , as also noted by Grundy et al. (1999). We used the Voyager albedo at  $0.9 \mu\text{m}$  of  $1.03(\pm 0.03)$  of Buratti et al. (1998) to set the scale on the ordinate. Note in particular that the continuum slope at the short wavelengths in the trailing hemisphere spectrum from 1998 is less steep than that of the leading hemisphere, also in accord with the spectra published by Grundy et al. (1999). No absorption features other than those of  $\text{H}_2\text{O}$  ice are evident.

### 3.3. Hyperion

While the appearance of the  $1.65\text{-}\mu\text{m}$   $\text{H}_2\text{O}$  band in the spectrum of Hyperion appears normal, the shape of the spectrum between  $1.70$  and  $1.85 \mu\text{m}$  is flatter than that of some other satellites. There are *significant differences* in the slopes among the spectra of the satellites in this region, as can be seen in Figs. 8 and 9. To illustrate one case, in Fig. 13 we show the spectra of Dione and Hyperion (both from

1995 September 9), normalized to give a good match in the 1.55  $\mu\text{m}$  band. The ratio of Hyperion to Dione shows the nature of the difference, possibly defining additional absorption in the Hyperion spectrum, centered at 1.75  $\mu\text{m}$ .

The difference appears to be real, and may be related to an absorption band in some unidentified component of the surfaces of the satellites. Methane ice absorbs in this region, but is ruled out by the lack of stronger bands at 2.2 and 2.3  $\mu\text{m}$ . Some of the tholins listed in Table 3 have minor absorption bands near this region (Cruikshank et al., 1991, Fig. 2), but are probably too weak to account for the differences among the satellites. Reference to the plot (Fig. 3) of the imaginary refractive index,  $k$ , of the two tholins we used will show that there is no significant absorption in either one of them at 1.8  $\mu\text{m}$ . Solid hydrocarbon complexes have combination and overtone bands in this region, with the first overtones and combinations of  $-\text{CH}_2$  and  $-\text{CH}_3$  occurring in the 1.69–1.76  $\mu\text{m}$  region in terrestrial bitumens (Cloutis et al., 1994; Moroz et al., 1998). Complex hydrocarbons may indeed be present on Hyperion, contributing to its lower albedo than most of Saturn's other icy satellites. The test of this possibility will come with the VIMS data from the Cassini–Huygens mission, which will cover the 3.4  $\mu\text{m}$  region where the  $-\text{CH}_2$  and  $-\text{CH}_3$  stretching mode fundamentals occur.

The absorption coefficients for hexagonal  $\text{H}_2\text{O}$  ice in the temperature range 70–120 K shown by Grundy and Schmitt (1998, Fig. 2) show differences in the slope of the absorption profile in the spectral region in question, but the difference in temperatures of Hyperion and Dione, and the other satellites presented here, are probably too small for the observed slope variations to be a temperature effect. This region in the spectra of Saturn's satellites requires further investigation.

### 3.4. Tethys and Dione

Our spectra shown in Figs. 8–10 do not show any features except  $\text{H}_2\text{O}$  ice absorption bands, and appear to be fully consistent with the spectra of Grundy et al. (1999). Because they are not obviously spectrally distinguished in other ways, we do not discuss them further.

## 4. Summary and conclusions

We have observed Saturn's icy satellites Mimas, Enceladus, Tethys, Dione, Rhea, and Hyperion in the spectral region 0.8–2.5  $\mu\text{m}$ , with data extending to 3.05  $\mu\text{m}$  for Tethys and to 3.6  $\mu\text{m}$  for Rhea (leading hemisphere) and Dione (trailing hemisphere). We have modeled the composite spectrum of Rhea, 0.3–3.6  $\mu\text{m}$ , using the Hapke and Shkuratov codes, finding that a fit to the entire spectrum is elusive. While crystalline (hexagonal)  $\text{H}_2\text{O}$  ice is the fundamental surface constituent, the absorption in the photovisual spectral region (0.3–1  $\mu\text{m}$ ) requires an additional component. We find that the addition of a very small quantity of a complex organic solid in the form of tholin provides the color in the

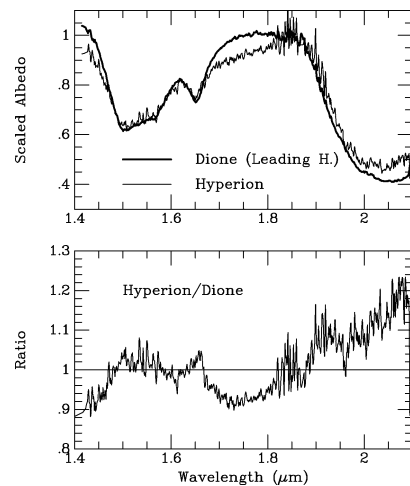


Fig. 13. (Top) Spectra of Dione and Hyperion (1995), normalized at 1.6  $\mu\text{m}$ . (Bottom) Ratio of Hyperion to Dione.

ultraviolet and photovisual regions, and is consistent with the appearance of the remainder of the spectrum. Our use of tholin in this regard is consistent with the results of Cuzzi and Estrada (1998), Poulet and Cuzzi (2002), and Poulet et al. (2003) in their models of Saturn's rings. Organic material in the icy surfaces of Rhea, the other satellites, and the rings, might originate from the infall of micrometeoroids (debris from comets or collisions in the Kuiper belt), or might be generated within the icy surfaces by the interaction of molecular impurities in the ice with solar ultraviolet radiation, cosmic rays, or atomic particles trapped in Saturn's magnetic field. The leading and trailing hemispheres of Mimas show the 1.65  $\mu\text{m}$  absorption band indicative of crystalline  $\text{H}_2\text{O}$  ice. We find no absorption bands attributable to ices other than  $\text{H}_2\text{O}$  on any of the satellites, although the spectrum of Hyperion shows a broad, unidentified absorption band centered at 1.75  $\mu\text{m}$ .

## Acknowledgments

We thank Dr. Will Grundy and his colleagues for supplying his spectra of the Saturn satellites (Grundy et al., 1999) in advance of publication, and Dr. Paul Estrada for a discussion of effective medium theory. Ms. Mary Jane Bartholomew contributed to an early phase of this work. We thank the support staff of UKIRT for its assistance in accomplishing some of the observations reported here. The United Kingdom Infrared Telescope is operated by the Joint Astronomy Centre on behalf of the U.K. Particle Physics and Astronomy Research Council. Cruikshank and Dalle Ore acknowledge partial support by NASA's Planetary Astronomy program (RTOP 344-32-20-01). Geballe is supported by the Gemini Observatory, which is operated by the Association of Universities for Research in Astronomy, Inc., on behalf of the international Gemini partnership of Argentina, Australia, Brazil, Canada, Chile, the United Kingdom, and the United States of America. Roush acknowledges support

from NASA's Planetary Geology and Geophysics program. We thank the management and staff of the NASA Infrared Telescope Facility for their support of this work.

### Appendix A. Determination of spectral geometric albedos of the Saturn satellites

As noted in the text, the spectra reported here were assembled by piecing together data obtained in increments of spectral coverage that varied with instrument and telescope, and with time. The CGS4 spectrometer on the United Kingdom Infrared Telescope, for example, was at different times configured with a variety of gratings with different dispersions and camera optics with different focal lengths.

Preceding or following each spectrum of one of the satellites, a solar-type star, or near solar-type star was observed at the same or very similar (within  $\sim 0.1$ ) airmass. Typical near-solar type stars included BS 6836 (G0V), BS 6998 (G4V), BS 88 (G2V), BS 582 (G2IV), and BS 7994 (G1V). The measured spectrum of the satellite was divided by the stellar spectrum and then multiplied by the flux of a blackbody at a temperature corresponding to the spectral type of the standard star. This produced the measured flux of the satellite in standard flux units. To convert these flux units to geometric albedo, we divided the flux of the satellite by the flux of the Sun given by Colina et al. (1996) ( $\lambda \leq 2.5 \mu\text{m}$ ) or Smith and Gottlieb (1974) ( $\lambda > 2.5 \mu\text{m}$ ) and then multiplied by the quantity  $R^2 * D^2 / r^2$ , where  $R$  and  $D$  are the heliocentric and geocentric distances of Saturn, respectively, and  $r$  is the radius of the satellite. No corrections for solar phase angle were made; all observations were made at small solar phase angles.

This method of calculating geometric albedo relies upon the assumption that *all* of the light from the satellite is included in the measurement. However, because all of the data were obtained with spectrometers using entrance slits, there is typically some loss of light because of seeing fluctuations, image drift, etc.; all such effects tend to reduce the measured flux and result in a lower calculated value for the albedo.

In view of this limitation on the geometric albedo calculation across the full spectrum, and because we found that some of the segments of the spectrum of a given satellite did not overlap (in geometric albedo) perfectly, we elected to assemble the spectral segments by reference to photometric determinations of the geometric albedo at standard filter-band wavelengths (e.g., UBVR<sub>I</sub>JHK), where such information is available. An additional important factor is that most of the objects observed here show asymmetries in brightness with their position in their orbits because of variations on their surfaces. Hyperion presents the additional variables of an irregular shape and a non-synchronous (chaotic) revolution/rotation. Where we show the spectra of Hyperion in this paper, we accept the observed flux and make no further corrections.

Corrections for the lightcurve variations of the satellites were made using the Earth-based data of Blair and Owen (1974), Noland et al. (1974), Franz and Millis (1975), and Verbiscer and Veverka (1989). The photometric framework for adjustment of the geometric albedo of each observed segment of the spectrum of a given satellite was derived from data given in the above references, plus Cruikshank (1979, 1980), Clark et al. (1984), Degewij et al. (1980), Buratti et al. (1998), and Momary et al. (2000), while the *relative* albedo levels at various wavelengths were in part derived from spectra by Grundy et al. (1999).

### References

- Bauer, J.M., Roush, T.L., Geballe, T.R., Meech, K.J., Owen, T.C., Vacca, W.D., Rayner, J.T., Jim, K.T.C., 2002. The near infrared spectrum of Miranda. *Icarus* 158, 178–190.
- Benedix, G.K., Roush, T.L., Owen, T.C., Cruikshank, D.P., Geballe, T.R., Dalle Ore, C.M., Khare, B.N., de Bergh, C., 1998. Surface composition models of the leading surfaces of Rhea and Dione. *Bull. Am. Astron. Soc.* 30, 1101. Abstract.
- Blair, G.N., Owen, F.N., 1974. The UVB orbital phase curves of Rhea, Dione, and Tethys. *Icarus* 22, 224–229.
- Bohn, R.B., Sandford, S.A., Allamandola, L.A., Cruikshank, D.P., 1994. Infrared spectroscopy of Triton and Pluto ice analogs: the case for saturated hydrocarbons. *Icarus* 111, 151–173.
- Bohren, C.F., Huffman, D.R., 1983. *Absorption and Scattering of Light by Small Particles*. Wiley, New York.
- Brown, M.E., 2000. Near-infrared spectroscopy of Centaurs and irregular satellites. *Astron. J.* 119, 977–983.
- Brown, M.E., Calvin, W.M., 2000. Evidence for crystalline water and ammonia ices on Pluto's satellite Charon. *Science* 287, 107–109.
- Brown, R.H., Cruikshank, D.P., Tokunaga, A.T., Smith, R.G., Clark, R.N., 1988. Search for volatiles on icy satellites. I. Europa. *Icarus* 74, 262–271.
- Buie, M.W., Grundy, W.M., 2000. The distribution and physical state of H<sub>2</sub>O on Charon. *Icarus* 148, 324–339.
- Buratti, B.J., Mosher, J.A., Johnson, T.V., 1990. Albedo and color maps of the saturnian satellites. *Icarus* 87, 339–357.
- Buratti, B.J., Mosher, J.A., Nicholson, P.D., McGhee, C.A., French, R.G., 1998. Near-infrared photometry of the saturnian satellites during ring plane crossing. *Icarus* 136, 223–231.
- Calvin, W.M., Clark, R.N., 1991. Modeling the reflectance spectrum of Callisto 0.25–4.1  $\mu\text{m}$ . *Icarus* 89, 305–317.
- Carlson, R.W., 13 colleagues, 1999. Hydrogen peroxide on the surface of Europa. *Science* 283, 2062–2064.
- Clark, R.N., Roush, T.L., 1984. Reflectance spectroscopy—quantitative analysis techniques for remote sensing applications. *J. Geophys. Res.* 89, 6329–6340.
- Clark, R.N., Brown, R.H., Owensby, P.D., Steele, A., 1984. Saturn's satellites: near-infrared spectrophotometry (0.65–2.5  $\mu\text{m}$ ) of the leading and trailing sides and compositional implications. *Icarus* 58, 265–281.
- Clark, R.N., Fanale, F.P., Gaffey, M.J., 1986. Surface composition of natural satellites. In: Burns, J.A., Matthews, M.S. (Eds.), *Satellites*. Univ. of Arizona Press, Tucson, pp. 437–491.
- Clark, R.N., Swayze, G.A., Gallagher, A.J., King, T.V.V., Calvin, W.M., 1993. U.S. Geological Survey, Digital Spectral Library: Version 1: 0.2 to 3.0 microns. U.S. Geological Survey Open File Report 93-592, 1340 pages, <http://speclab.cr.usgs.gov>.
- Cloutis, E.A., Gaffey, M.J., Moslow, T.F., 1994. Spectral reflectance properties of carbon-bearing materials. *Icarus* 107, 276–287.
- Colina, L., Bohlin, R.C., Castelli, F., 1996. The 0.12–2.5  $\mu\text{m}$  absolute flux distribution of the Sun for comparison with solar analog stars. *Astron. J.* 112, 307–315.

- Cruikshank, D.P., 1979. The surfaces and interiors of the satellites of Saturn. *Rev. Geophys. Space Phys.* 17, 165–176.
- Cruikshank, D.P., 1980. Near-infrared studies of the satellites of Saturn and Uranus. *Icarus* 41, 246–258.
- Cruikshank, D.P., Lebofsky, L.A., Veverka, J., 1984. Satellites of Saturn: optical properties. In: Gehrels, T., Matthews, M.S. (Eds.), *Saturn*. Univ. of Arizona Press, Tucson, pp. 640–667.
- Cruikshank, D.P., Allamandola, L.J., Hartmann, W.K., Tholen, D.J., Brown, R.H., Matthews, C.N., Bell, J.F., 1991. Solid C≡N bearing material on outer Solar System bodies. *Icarus* 94, 345–353.
- Cruikshank, D.P., Roush, T.L., Owen, T.C., Geballe, T.R., de Bergh, C., Schmitt, B., Brown, R.H., Bartholomew, M.J., 1993. Ices on the surface of Triton. *Science* 261, 742–745.
- Cruikshank, D.P., Brown, R.H., Calvin, W., Roush, T.L., Bartholomew, M.J., 1998a. Ices on the satellites of Jupiter, Saturn, and Uranus. In: Schmitt, B., de Bergh, C., Festou, M. (Eds.), *Solar System Ices*. Kluwer Academic, Dordrecht, pp. 579–606.
- Cruikshank, D.P., Roush, T.L., Owen, T.C., Quirico, E., de Bergh, C., 1998b. The surface compositions of Triton, Pluto, and Charon. In: Schmitt, B., de Bergh, C., Festou, M. (Eds.), *Solar System Ices*. Kluwer Academic, Dordrecht, pp. 655–684.
- Cruikshank, D.P., Roush, T.L., Bartholomew, M.J., Geballe, T.R., Pendleton, Y.J., White, S.M., Bell III, J.F., Davies, J.K., Owen, T.C., de Bergh, C., Tholen, D.J., Bernstein, M.P., Brown, R.H., Tryka, K.A., Dalle Ore, C.M., 1998c. The composition of Centaur 5145 Pholus. *Icarus* 135, 389–407.
- Cruikshank, D.P., Schmitt, B., Roush, T.L., Owen, T.C., Quirico, E., Geballe, T.R., de Bergh, C., Bartholomew, M.J., Dalle Ore, C.M., Douté, S., Meier, R., 2000. Water ice on Triton. *Icarus* 147, 309–316.
- Cruikshank, D.P., Roush, T.L., Poulet, F., 2003. Quantitative modeling of the spectral reflectance of Kuiper belt objects and Centaurs. *C. R. Phys.* 4, 783–789.
- Cuzzi, J.N., Estrada, P.R., 1998. Compositional evolution of Saturn's rings due to meteoroid bombardment. *Icarus* 132, 1–35.
- Dalle Ore, C.M., Cruikshank, D.P., Owen, T.C., Geballe, T.R., Roush, T.L., Khare, B.N., de Bergh, C., 1999. Surface composition of Rhea from reflectance spectra, 0.2–3.6  $\mu\text{m}$ . *Bull. Am. Astron. Soc.* 31, 1073. Abstract.
- Davies, J.K., Roush, T.L., Cruikshank, D.P., Bartholomew, M.J., Geballe, T.R., Owen, T., de Bergh, C., 1997. The detection of water ice in Comet Hale–Bopp. *Icarus* 127, 238–245.
- Degewij, J., Cruikshank, D.P., Hartmann, W.K., 1980. Near-infrared colorimetry of J6 Himalia and S9 Phoebe: a summary of 0.3–2.2  $\mu\text{m}$  reflectances. *Icarus* 44, 542–547.
- Delitsky, M.L., Lane, A.L., 2002. Saturn's inner satellites: ice chemistry and magnetosphere effects. *J. Geophys. Res.* 107 (E11), 5093, 3-1–3-17.
- Douté, S., Schmitt, B., Quirico, E., Owen, T.C., Cruikshank, D.P., de Bergh, C., Geballe, T.R., Roush, T.R., 1999. Evidence for methane segregation at the surface of Pluto. *Icarus* 142, 421–444.
- Fink, U., Larson, H.P., 1975. Temperature dependence of the water-ice spectrum between 1 and 4 microns: application to Europa, Ganymede, and Saturn's rings. *Icarus* 24, 411–420.
- Fink, U., Sill, G.T., 1982. The infrared spectral properties of frozen volatiles. In: Wilkening, L.L. (Ed.), *Comets*. Univ. of Arizona Press, Tucson, pp. 164–202.
- Fink, U., Larson, H.P., Gautier, T.N., Treffers, R.R., 1976. Infrared spectra of the satellites of Saturn: identification of water ice on Iapetus, Rhea, Dione, and Tethys. *Astrophys. J.* 207, L63–L67.
- Franz, O.G., Millis, R.L., 1975. Photometry of Dione, Tethys, and Enceladus on the UVB system. *Icarus* 24, 433–442.
- Grundy, W.M., Schmitt, B., 1998. The temperature-dependent near-infrared absorption spectrum of hexagonal H<sub>2</sub>O ice. *J. Geophys. Res.* 103, 25809–25822.
- Grundy, W.M., Buie, M.W., Stansberry, J.A., Spencer, J.R., 1999. Near-infrared spectra of outer Solar System surfaces: remote determination of H<sub>2</sub>O ice temperatures. *Icarus* 142, 536–549.
- Hapke, B., 1981. Bidirectional reflectance spectroscopy 1. Theory. *J. Geophys. Res.* 86, 3039–3054.
- Hapke, B., 1993. Combined theory of reflectance and emittance spectroscopy. In: Pieters, C.M., Englert, P.A.J. (Eds.), *Remote Geochemical Analysis: Elemental and Mineralogical Composition*. Cambridge Univ. Press, New York, pp. 31–42.
- Imanaka, H., Khare, B.N., Eilsa, J.E., Bakes, E.L.O., McKay, C.P., Cruikshank, D.P., Sugita, S., Matsui, T., Zare, R.N., 2004. Laboratory experiments on Titan tholin formed in cold plasma at various pressures: implications for nitrogen-containing polycyclic aromatic compounds in Titan haze. *Icarus* 168, 344–366.
- Khare, B.N., Sagan, C., Arakawa, E.T., Suits, R., Callcot, T.A., Williams, M.W., 1984. Optical constants of organic tholins produced in a simulated titanian atmosphere: from soft X-ray to microwave frequencies. *Icarus* 60, 127–137.
- Khare, B.N., Thompson, W.R., Cheng, L., Chyba, C., Sagan, C., Arakawa, E.T., Meisse, C., Tuminello, P., 1993. Production and optical constants of ice tholin from charged particle irradiation of (1:6) C<sub>2</sub>H<sub>6</sub>/H<sub>2</sub>O at 77 K. *Icarus* 103, 290–300.
- Kuiper, G.P., 1957. Infrared observations of planets and satellites. *Astron. J.* 62, 245. Abstract.
- Kuiper, G.P., Cruikshank, D.P., Fink, U., 1970. Letter to Editor. *Sky Telescope* 39, 80.
- Levy, O., Stroud, D., 1997. Maxwell Garnett theory for mixtures of anisotropic inclusions: application to conducting polymers. *Phys. Rev. B* 56, 8035–8046.
- Lucey, P.G., 1998. Model near-infrared optical constants of olivine and pyroxene as a function of iron content. *J. Geophys. Res.* 103, 1703–1713.
- Lupo, M.J., Lewis, J.S., 1979. Mass-radius relationships in icy satellites. *Icarus* 40, 157–170.
- McCord, T.B., the Galileo NIMS Team, 1998. Non-water-ice constituents in the surface material of the icy galilean satellites from the Galileo near-infrared mapping spectrometer investigation. *J. Geophys. Res.* 103, 8603–8616.
- McDonald, G.D., Thompson, W.R., Heinrich, M., Khare, B.N., Sagan, C., 1994. Chemical investigation of Titan and Triton tholins. *Icarus* 108, 137–145.
- McDonald, G.D., Whited, L.J., DeRuiter, C., Khare, B.N., Patniak, A., Sagan, C., 1996. Production and chemical analysis of cometary ice tholins. *Icarus* 122, 107–117.
- Momary, T.W., Baines, K.H., Yanamandra-Fisher, P.A., Lebofsky, L.A., Golisch, W., Kaminski, C., 2000. The saturnian satellites in the near-infrared: absolute photometry at ring plane crossing. *Icarus* 148, 397–406.
- Moroz, V.I., 1967. *Physika Planet. Nauka*, Moscow. 496 pp. In Russian.
- Moroz, L.V., Arnold, G., Korochantsev, A.V., Wasch, 1998. Natural solid bitumens as possible analogs for cometary and asteroid organics. *Icarus* 134, 253–268.
- Morrison, D., Owen, T., Soderblom, L.A., 1986. The satellites of Saturn. In: Burns, J.A., Matthews, M.S. (Eds.), *Satellites*. Univ. of Arizona Press, Tucson, pp. 764–801.
- Mosqueira, I., Estrada, P.R., 2003a. Formation of large regular satellites of giant planets in an extended gaseous nebula. I. Subnebula model and accretion of satellites. *Icarus* 163, 198–231.
- Mosqueira, I., Estrada, P.R., 2003b. Formation of large regular satellites of giant planets in an extended gaseous nebula. II. Satellite migration and survival. *Icarus* 163, 232–255.
- Mountain, C.M., Robertson, D., Lee, T.J., Wade, R., 1990. An advanced cooled grating spectrometer for UKIRT. In: Crawford, D.L. (Ed.), *Proc. SPIE*, vol. 1235, pp. 25–33.
- Noland, M., Veverka, J., Morrison, D., Cruikshank, D.P., Lazarewicz, A.R., Morrison, N.D., Elliot, J.L., Goguen, J., Burns, J.A., 1974. Six-color photometry of Iapetus, Titan, Rhea, Dione and Tethys. *Icarus* 23, 334–354.
- Noll, K.S., Roush, T.L., Cruikshank, D.P., Pendleton, Y.J., Johnson, R.E., 1997. Detection of ozone on Saturn's satellites Rhea and Dione. *Nature* 388, 45–47.

- Owen, T.C., Cruikshank, D.P., Roush, T., de Bergh, C., Brown, R.H., Bartholomew, M.J., Elliot, J., Young, L., 1993. The surface ices and the atmospheric composition of Pluto. *Science* 261, 745–748.
- Owen, T.C., Cruikshank, D.P., Dalle Ore, C.M., Geballe, T.R., Roush, T.L., de Bergh, C., 1999. Detection of water ice on Saturn's satellite Phoebe. *Icarus* 139, 379–382.
- Owen, T.C., Cruikshank, D.P., Dalle Ore, C.M., Geballe, T.R., Roush, T.L., de Bergh, C., Pendleton, Y.J., Khare, B.N., 2001. Decoding the domino: the dark side of Iapetus. *Icarus* 149, 160–172.
- Piatek, J.L., Hapke, B., Nelson, R.M., Smythe, W.D., Hale, A.S., 2002. Scattering properties of planetary regolith analogs. *Lunar Planet. Sci.* 33. Abstract 1171 [CD-ROM].
- Piatek, J.L., Hapke, B., Nelson, R.M., Hale, A.S., Smythe, W.D., 2003. Size-dependent measurements of the scattering properties of planetary regolith analogs: a challenge to theory. *Lunar Planet. Sci.* 34. Abstract 1440 [CD-ROM].
- Pilcher, C.B., Chapman, C.R., Lebofsky, L.A., Kieffer, H.H., 1970. Saturn's rings: identification of water frost. *Science* 167, 1372–1373.
- Poulet, F., Cuzzi, J.N., 2002. The composition of Saturn's rings. *Icarus* 160, 350–358.
- Poulet, F., Cuzzi, J.N., Cruikshank, D.P., Roush, T., Dalle Ore, C.M., 2002. Comparison between the Shkuratov and Hapke scattering theories for solid planetary surfaces. Application to the surface composition of two centaurs. *Icarus* 160, 313–324.
- Poulet, F., Cruikshank, D.P., Cuzzi, J.N., Roush, T.L., French, R.G., 2003. Compositions of Saturn's rings A, B, and C from high spectral resolution near-infrared spectroscopic observations. *Astron. Astrophys.* 412, 305–316.
- Prinn, R.G., Fegley Jr., B., 1981. Kinetic inhibition of CO and N<sub>2</sub> reduction in circumplanetary nebulae—implications for satellite composition. *Astrophys. J.* 249, 308–317.
- Quirico, E., Schmitt, B., 1997. Near-infrared spectroscopy of simple hydrocarbons and carbon oxides diluted in solid N<sub>2</sub> and as pure ices: implications for Triton and Pluto. *Icarus* 127, 354–378.
- Quirico, E., Douté, S., Schmitt, B., de Bergh, C., Cruikshank, D.P., Owen, T.C., Geballe, T.R., Roush, T.L., 1999. Composition, physical state and distribution of ices at the surface of Triton. *Icarus* 139, 159–178.
- Rayner, J.T., Toomey, D., Onaka, P.M., Denault, A.J., Stahlberger, W.E., Vacca, W.D., Cushing, M.C., Wang, S., 2003. SpeX: a medium-resolution 0.8–5.5 micron spectrograph and imager for the NASA infrared telescope facility. *Publ. Astron. Soc. Pacific* 115, 362–382.
- Ramirez, S.I., Coll, P., da Silva, A., Navarro-González, R., Lafait, L., Raulin, F., 2002. Complex refractive index of Titan's aerosol analogues in the 200–900 nm domain. *Icarus* 156, 515–529.
- Roddiér, F., Roddiér, C., Brahic, A., Dumas, C., Graves, J.E., Northcott, M.J., Owen, T., 2000. Adaptive optics observations of Saturn's ring plane crossing in August 1995. *Icarus* 143, 299–307.
- Roush, T.L., 1994. Charon: more than water ice? *Icarus* 108, 243–254.
- Roush, T.L., Cruikshank, D.P., Owen, T.C., 1995. Surface ices in the outer Solar System. In: Farley, K.A. (Ed.), *Volatiles in the Earth and Solar System*. In: *Am. Inst. Phys. Conf. Proc.*, vol. 341, pp. 143–153.
- Schmitt, B., Quirico, E., Trotta, F., Grundy, W.M., 1998. Optical properties of ices from UV to infrared. In: Schmitt, B., de Bergh, C., Festou, M. (Eds.), *Solar System Ices*. Kluwer Academic, Dordrecht, pp. 199–240.
- Schubert, G., Spohn, T., Reynolds, R.T., 1986. Thermal histories, compositions and internal structures of the moons of the Solar System. In: Burns, J.A., Matthews, M.S. (Eds.), *Satellites*. Univ. of Arizona Press, Tucson, pp. 224–292.
- Shkuratov, Y., Starukhina, Y., Hoffmann, H., Arnold, G., 1999. A model of spectral albedo of particulate surfaces: implications for optical properties of the Moon. *Icarus* 137, 235–246.
- Sill, G., Fink, U., Ferraro, J.R., 1980. Absorption coefficients of solid NH<sub>3</sub> from 50 to 7000 cm<sup>-1</sup>. *J. Opt. Soc. Am.* 70, 724–739.
- Sill, G., Fink, U., Ferraro, J.R., 1981. The infrared spectrum of ammonia hydrate: explanation for a reported ammonia phase. *J. Chem. Phys.* 74, 997–1000.
- Slobodkin, L.S., Buyakov, I.F., Cess, R.D., Caldwell, J., 1978. Near infrared reflection spectra of ammonia frost: interpretation of the upper clouds of Saturn. *J. Quant. Spectrosc. Radiat. Transfer* 20, 481–490.
- Smith, E.V.P., Gottlieb, D.M., 1974. Solar flux and its variations. *Space Sci. Rev.* 16, 771–802.
- Smith, B.A., the Voyager Imaging Team, 1981. Encounter with Saturn: Voyager 1 imaging science results. *Science* 212, 163–191.
- Tokunaga, A.T., 2000. Infrared astronomy. In: Cox, A.N. (Ed.), *Allen's Astrophysical Quantities*. Springer-Verlag, New York, pp. 143–167.
- Tran, B.N., Ferris, J.P., Chera, J.J., 2003. The photochemical formation of a Titan haze analog. Structural analysis by X-ray photoelectron and infrared spectroscopy. *Icarus* 162, 114–124.
- Verbiscer, A.J., Veverka, J., 1989. Albedo dichotomy of Rhea: Hapke analysis of Voyager photometry. *Icarus* 82, 336–353.
- Wilson, P.D., Sagan, C., Thompson, W.R., 1994. The organic surface of 5145 Pholus: constraints set by scattering theory. *Icarus* 107, 288–303.